Journal Pre-proof

PLSCR1 Promotes Apoptosis and Clearance of Retinal Ganglion Cells in Glaucoma Pathogenesis

Jingyi Luo, Qing Lian, Deliang Zhu, Minglei Zhao, Tingfang Mei, Bizhi Shang, Zeqiu Yang, Chujun Liu, Wenchang Xu, Lan Zhou, Keling Wu, Xinqi Liu, Yuhua Lai, Fuxiang Mao, Weihua Li, Chengguo Zuo, Kang Zhang, Mingkai Lin, Yehong Zhuo, Yizhi Liu, Lin Lu, Ling Zhao
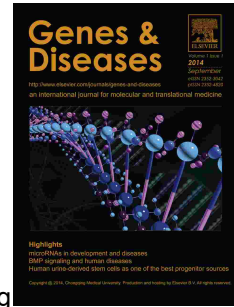
Please cite this article as: Luo J, Lian Q, Zhu D, Zhao M, Mei T, Shang B, Yang Z, Liu C, Xu W, Zhou L, Wu K, Liu X, Lai Y, Mao F, Li W, Zuo C, Zhang K, Lin M, Zhuo Y, Liu Y, Lu L, Zhao L, PLSCR1 Promotes Apoptosis and Clearance of Retinal Ganglion Cells in Glaucoma Pathogenesis, *Genes & Diseases*, https://doi.org/10.1016/j.gendis.2022.05.036.

This is a PDF file of an article that has undergone enhancements after acceptance, such as the addition of a cover page and metadata, and formatting for readability, but it is not yet the definitive version of record. This version will undergo additional copyediting, typesetting and review before it is published in its final form, but we are providing this version to give early visibility of the article. Please note that, during the production process, errors may be discovered which could affect the content, and all legal disclaimers that apply to the journal pertain.

PLSCR1 Promotes Apoptosis and Clearance of Retinal Ganglion Cells in Glaucoma Pathogenesis

Jingyi Luo[a,1], Qing Lian[a,b,1], Deliang Zhu[a,c,1], Minglei Zhao[a], Tingfang Mei[a], Bizhi Shang[a], Zeqiu Yang[a], Chujun Liu[a], Wenchang Xu[a], Lan Zhou[d], Keling Wu[a], Xinqi Liu[a,e], Yuhua Lai[a], Fuxiang Mao[a], Weihua Li[a], Chengguo Zuo[a], Kang Zhang[f], Mingkai Lin[a], Yehong Zhuo[a], Yizhi Liu[a,g,h*], Lin Lu[a*], Ling Zhao[a,2*]

[a]State Key Laboratory of Ophthalmology, Zhongshan Ophthalmic Center, Sun Yat-sen University, Guangdong Provincial Key Laboratory of Ophthalmology and Visual Science, Guangzhou, 510060, PR China

[b]Dongguan Guangming Ophthalmic Hospital, Dongguan, Guangdong 523000, PR China

[c]Guangdong Provincial People's Hospital, Guangdong Academy of Medical Sciences, Guangzhou, 510080, PR China

[d]Department of Ophthalmology, Huizhou Municipal Central Hospital, Huizhou, 516000, PR China

[e]Guangdong Province Key Laboratory of Brain Function and Disease, Zhongshan School of Medicine, Sun Yat-sen University, Guangzhou, 510000, PR China

[f]Center for Biomedicine and Innovations, Faculty of Medicine, Macau University of Science and Technology, Macau, 999078, PR China

[g]Guangzhou Regenerative Medicine and Health Guangdong Laboratory, Guangzhou, 510530, PR China

[h]Research Unit of Ocular Development and Regeneration, Chinese Academy of

Medical Sciences, Guangzhou, 510060, PR China

[1]These authors contributed equally

[2]Lead contact

*Corresponding authors:

Ling Zhao, PhD

Professor of Ophthalmology

State Key Laboratory of Ophthalmology, Zhongshan Ophthalmic Center, Sun Yat-sen University, Guangzhou 510060, PR China

E-mail: zhaoling6@mail.sysu.edu.cn

Lin Lu, MD, PhD

Professor, Director, Fundus Disease Center

State Key Laboratory of Ophthalmology, Zhongshan Ophthalmic Center, Sun Yat-sen University, Guangzhou 510060, PR China

E-mail: drlulin@126.com

Yizhi Liu, MD, PhD

Professor, Director

State Key Laboratory of Ophthalmology, Zhongshan Ophthalmic Center, Sun Yat-sen University, Guangzhou 510060, PR China

E-mail: yzliu62@yahoo.com

Declarations of interest: none

Authors email address:

Jingyi Luo: camel043@126.com

Qing lian: lianqing5678@163.com

Deliang Zhu: zhudeliang2014@163.com

Minglei Zhao: zhaoml09@163.com

Tingfang Mei: mtfgibh@163.com

Bizhi Shang: shangbizhi@126.com

Zeqiu Yang: yangzeqiu123@163.com

Chujun Liu: liuchujun@hotmail.com

Wenchang Xu: xwj8944@163.com

Lan Zhou: zhoulanvin@163.com

Keling Wu: wklkaren@foxmail.com

Xinqi Liu: gztszcg@163.com

Yuhua Lai: laiyuhuazd@163.com

Fuxiang Mao: 807253341@qq.com

Weihua Li: wei-yu1106@163.com

Chengguo Zuo: chengguozuo@163.com

Kang Zhang: kang.zhang@gmail.com

Mingkai Lin: linmk@mail.sysu.edu.cn

Yehong Zhuo: zhuoyh@mail.sysu.edu.cn

Yizhi Liu: yzliu62@yahoo.com

Lin Lu: drlulin@126.com

Ling Zhao: zhaoling6@mail.sysu.edu.cn

1 **Abstract**

2 Glaucoma is the leading cause of irreversible blindness worldwide. In the pathogenesis

3 of glaucoma, activated microglia can lead to retinal ganglion cells (RGCs) apoptosis

4 and death, however, the molecular mechanisms remain largely unknown. We

5 demonstrate that phospholipid scramblase 1 (PLSCR1) is a key regulator promoting

6 RGCs apoptosis and their clearance by microglia. As evidenced in retinal progenitor

7 cells and in RGCs of the acute ocular hypertension (AOH) mouse model,

8 overexpressed PLSCR1 induced its translocation from the nucleus to the cytoplasm

9 and cytomembrane, as well as elevated phosphatidylserine exposure and reactive

10 oxygen species generation with subsequent RGCs apoptosis and death. These

11 damages were effectively attenuated by PLSCR1 inhibition. In the AOH model,

12 PLSCR1 leads to an increase in M1 type microglia activation and retinal

13 neuroinflammation. Upregulation of PLSCR1 results in strongly elevated phagocytosis

14 of apoptotic RGCs by activated microglia. Taken together, our study provides important

15 insights linking activated microglia to RGCs death in the glaucoma pathogenesis and

16 other RGC-related neurodegenerative diseases.

17

18 **Keywords**

19 Apoptosis; Glaucoma; Phagocytosis; PLSCR1; Retinal ganglion cells.

20

21 **Abbreviations**

22

23 AOH, acute ocular hypertension; CNS, central nervous system; DAPI, 4 ,6-diamidino-

24 2-phenylindole; DCFH-DA, 2',7'-dichlorodihydrofluorescein diacetate; DHE,

25 dihydroethidium; GCL, ganglion cell layer; H&E, hematoxylin and eosin; hiPSCs,

26 human induced pluripotent stem cells; Iba-1, ionized calcium-binding adaptor molecule

27 1; INL, inner nuclear layer; IOP, intraocular pressure; IPL, inner plexiform layer; OGDR,

28 oxygen and glucose deprivation/reoxygenation; ONC, optic nerve crush; ONL, outer

29 nuclear layer; OPL, outer plexiform layer; PFA, paraformaldehyde; PI, propidium iodide;

30 PLSCR1, phospholipid scramblase 1; PS, phosphatidylserine; pSIVA, polarity

31 sensitive indicator of viability and apoptosis; qPCR, quantitative polymerase chain

32 reaction; RGCs, retinal ganglion cells; ROS, reactive oxygen species; RPCs, retinal

33 progenitor cells; RT, room temperature; RT-PCR, real-time reverse transcription-

34 polymerase chain reaction; siRNA, small interfering RNA; TB, toluidine blue; TG,

35 transgenic; TUNEL, terminal deoxynucleotidyl transferase biotin-UTP nick end labeling.

36 WT, wild-type.

37

Background

39 Glaucoma, the leading cause of irreversible blindness worldwide, is characterized by

40 progressive retinal ganglion cells (RGCs) degeneration and death and impairment of

41 visual function.[1-3] The pathogenesis of RGCs degeneration and death is complex. The

42 pathophysiology of glaucomatous damage is multifactorial and not completely

43 understood. Activation of retinal microglia has been found to promote RGCs apoptosis

44 and death in the pathogenesis of glaucoma.[4,5] However, the underlying molecular

45 mechanisms are still largely unknown.

46 Microglia are resident immune cells in the human and rodent retina.[6] In physiological

47 conditions, microglia are located in the ganglion cell layer (GCL), inner plexiform layer

48 (IPL), and outer plexiform layer (OPL) with ramified morphology.[4] In inherited

49 photoreceptor degeneration, activated microglia could facilitate rod death via

50 phagocytosis and secretion of IL-1 .[7] In the glaucomatous retina, activated microglia

51 could progressively migrate to GCL, which is thought to be deleterious in the process

52 of retinal degeneration.[4]

53   Recent studies indicate that lipid metabolism and turnover play a critical role in the

54 pathogenesis of glaucoma.[8,9] Phospholipid scramblase 1 (PLSCR1) is a calcium-

55 dependent type II single-pass transmembrane protein. Activation of PLSCR1 promotes

56 phosphatidylserine (PS) to expose from the inner leaflet to the outer leaflet of plasma

57 membrane, which is one of the characteristics of early apoptosis and as an "eat-me"

58 signal for microglia to recognize and engulf stressed cells.[10,11] PLSCR1 might be

59 associated with neuron death, as increased PLSCR1-immunoreactive neurons were

60 observed in the human hippocampus after cerebral ischemia.[12] Though downregulated

61 expression of PLSCR1 could inhibit microglial activation for the clearance of virus

62 transduced-astrocytes in the central nervous system (CNS),[13] it has not been

63 investigated whether PLSCR1 is directly involved in the microglia activation and

64 neuron death.

65   In this study, we explored the connection between PLSCR1 and retinal microglia,

66 and revealed their relationships with RGCs death. Our study points out that PLSCR1

67 is a pivotal regulator promoting RGCs apoptosis and their clearance by activated retinal

68 microglia. Our findings provide novel insights into the mechanisms of microglial

69 activation in glaucoma pathogenesis, which might contribute to potential therapeutic

70 interventions for glaucoma and other RGC-related neurodegenerative diseases.

71

72 **Materials and Methods**

73 **Reagents and resources**

74 The detailed information on reagents and resources, including antibodies, chemicals,

75 sequences, and other materials related to our study are listed in the Supplementary

76 Information.

77

78 **Retinal progenitor cells (RPCs) and cell culture**

79 Human induced pluripotent stem cells (hiPSCs) were purchased from Saibei company

80 (Beijing, China). The procedure of hiPSCs differentiation into RPCs was modified as

81 previously described.[14] Briefly, hiPSCs were cultured using retinal induced medium

82 (RIM) in a 12-well culture plate for five days. RIM was change every day. From the

83 sixth day, hiPSCs were cultured using the retinal differentiation medium (RDM) for

84 seven days. From day 12, the cells were transplanted to the retinal progenitor cell

85 differentiation medium (RPCDM). The RPC-like cells were mechanically enriched by

86 scraping out with non-RPC morphology. Enriched RPCs were cultured in retinal

87 progenitor cell medium (RPCM) for three days. Then the RPCs were cultured in

88 Dulbecco's modified Eagle's medium/nutrient mixture F-12 (DMEM/F12)

89 supplemented with 10% fetal bovine serum (FBS) and maintained at 37 °C in an

90 incubator at 5% CO_2. The hiPSCs exhibited typical clonal morphology and were

91 characterized by traditional pluripotent stem cell markers OCT4, Tra-1-60, while RPCs

92 differentiated from hiPSCs were characterized by Pax6, Nestin, CHX10, and LHX2.

93 Flow cytometry was applied to validate differentiation efficiency from hiPSCs to RPCs

94 (Fig. S1). The detailed composition of the cell culture medium was listed in

95 Supplementary information.

96

97 **Adenoviral transfection and RNA interference**

98 For the adenoviral transfection, the adenovirus packaging expressing PLSCR1 (pAd-

4

99 PLSCR1) and the control (pAd-NC) vector were obtained from Vigene Biosciences

100 Company (Shandong, China). All the plasmids were verified by DNA sequencing. The

101 adenoviruses were added into the RPC culture medium at a multiplicity of infection

102 (MOI) of 30.

103 For the RNA interference, effective small interfering RNA (siRNA) targeting human

104 PLSCR1 (si-PLSCR1) and a negative control scrambled siRNA (si-NC) were

105 purchased from GenePharma Company (Shanghai, China) and transfected using

106 Lipofectamine® RNAiMax (Invitrogen, USA) according to the manufacturer's

107 instructions. The transfection was conducted 24 h prior to oxygen and glucose

108 deprivation/reoxygenation (OGDR) treatment. The expression levels of PLSCR1 were

109 verified by Western blot. The sequences used were listed in the Supplementary

110 Information.

111

112 **OGDR model**

113 To establish the OGDR model, the culture medium of RPCs was replaced with glucose-

114 free DMEM (Gibco) after washing cells twice with PBS. Then, the cells were placed in

115 a 5% CO_2 and 95% N_2 atmospheric incubator chamber under hypoxic conditions for 3

116 h at 37 °C. After that, RPCs were cultured in the normal medium again and maintained

117 in a normoxic (5% CO_2 and 95% air) atmospheric incubator for 24 h. Control groups

118 were cultured in the normal medium in a normoxic atmospheric incubator for the same

119 duration.

120

121 **Mice**

122 All the animal procedures were approved by the Animal Care and Ethics Committee of

123 Zhongshan Ophthalmic Center, Sun Yat-Sen University (Guangzhou, China), and all

124 the Use of Animals were performed in accordance with the Association for Research

125 in Vision and Ophthalmology (ARVO) statement. C57BL/6J wild-type (WT) mice and

126 transgenic PLSCR1 (TG-PLSCR1) mice produced on the C57BL/6J background were

127 generated from Gempharmatech Co., Ltd (Jiangsu, China). Two mouse lines showed

128 PLSCR1 overexpression in the retina identified by immunostaining and Western blot

129 were selected to further breeding. Mice aged from 4 to 6 weeks were examined in this

130 study. In all procedures, mice were weighed and anesthetized by intraperitoneal

131 injection of 1% pentobarbital sodium (50 mg/kg, Sigma, USA) and topically

132 anesthetized with 0.5% proparacaine hydrochloride eye drops (Alcon, USA). Their

133 pupils were dilated with topical administration of tropicamide phenylephrine eye drops

134 (Santen, Japan). Animals were maintained on a 12-h light-dark cycle and housed in

135 the Animal Laboratory of Zhongshan Ophthalmic Center.

136

137 **Acute ocular hypertension (AOH) mouse model**

138 The procedure of AOH model was carried out as our previous study described.[3] To

139 establish the AOH model, the WT mice and TG-PLSCR1 mice were anesthetized and

140 their pupils were dilated. The anterior chamber of the right eye was cannulated with a

141 30-gauge infusion needle connected to a 150-ml bottle of normal saline solution, which

142 was elevated to the height of 150 cm to maintain an IOP of 110 mmHg for 60 min. The

143 left eye without AOH was served as the control group. After the procedure, tobramycin

144 ointment (Alcon, USA) was applied to the eye surface for preventing postoperative

145 infection. Eyes without cataracts, iris injury/bleeding, anterior chamber leakage, or

146 infections were collected for further study.

147

148 **Optic nerve crush (ONC) injury mouse model**

149   The ONC surgery was performed as previously described.[15] After general and topical

150   anesthetization, a small incision was made in the superior-external conjunctiva and

151   orbital muscles were gently put aside with fine forceps (Dumont #5B, WPI, USA) to

152   expose the optic nerve. The optic nerve was clamped with self-clamping forceps at

153   about 1.5 mm behind the eye globe for three seconds. The left eye without crushing

154   served as control. Eyes were harvested on the fifth day after treatment.

155

156   **Western blot analysis**

157   Western blot analysis was performed as previously described.[16] After extraction from

158   RPCs or mouse retinas, the concentrations of the proteins were measured. Equal

159   amounts of proteins were separated on 10% sodium dodecyl sulfate-polyacrylamide

160   gel electrophoresis resolving gel and 5% stacking gel and transferred onto

161   polyvinylidene fluoride (PVDF) membrane. PVDF membrane was blocked with 5%

162   skim milk in Tris-buffered saline plus 0.1% Tween-20 (TBST) for 1 h at room

163   temperature (RT), and then incubated with primary antibodies (rabbit anti-PLSCR1,

164   1:1000, Proteintech; rabbit anti-Tubulin,1:1000, Abcam) at 4 °C overnight. Then the

165   membranes were incubated with secondary antibodies (HRP-goat anti-rabbit IgG,

166   1:2000) for 2 h at RT. Proteins signals were developed with SuperSignal™ West Femto

167   Maximum Sensitivity Substrate (Thermos Fisher Scientific) and imaged using a

168   chemiluminescence system (Bio-Rad Laboratories, USA).

169

170   **Flow cytometry**

171   Cell apoptosis and reactive oxygen species (ROS) were detected by flow cytometric

172   analysis using Annexin V-FITC/PI and 2',7'-dichlorodihydrofluorescein diacetate

173   (DCFH-DA, Life Technologies, Thermo Fisher Scientific, USA), respectively.

174 Approximately 1×10^6 RPCs cultured in a 6-well plate were transfected with adenoviral

175 or siRNA for 48 to 72 h. The cells were digested by 0.25% trypsin, washed twice with

176 PBS, and then incubated with Annexin V-FITC/PI (Annexin V-FITC Apoptosis Detection

177 Kit, BD Biosciences, USA) or 10 μM DCFH-DA (Reactive Oxygen Species Assay Kit,

178 Beyotime, China) for 20 min. All groups in the experiment were repeated in triplicate.

179 Cell apoptosis and intracellular ROS level were detected by a flow cytometer (BD

180 Biosciences, USA). Data were analyzed by the BD FACSDiva 8.0.1.

181

182 **Immunofluorescence staining**

183 **In cells:** Cultured iPSCs and iPSC-RPCs were washed with PBS and fixed with 4%

184 paraformaldehyde (PFA) for 15 min, then washed twice with PBS. Then the cells were

185 incubated in 0.1M PBS containing 3% bovine serum albumin (BSA) and 0.5% Triton

186 X-100 at RT for 1 h. Followed by incubation with primary antibodies (rabbit anti-OCT4,

187 1:400; mouse anti-Tra-1-60, 1:200; rabbit anti-Pax6, 1:400; mouse anti-CHX10, 1:400;

188 mouse anti-LHX2, 1:400; rabbit anti-nestin, 1:400; rabbit anti-PLSCR1, 1:200)

189 overnight at 4 °C, cells were washed with PBS, and incubated with secondary

190 antibodies (1:500) and DAPI (1:5000). Images were captured with a confocal scanning

191 microscope LSM800 (Carl Zeiss, Germany).

192 **In tissues:** The mice were overdosed with anesthesia and transcardially perfused with

193 4% PFA and PBS. The eyes were enucleated and immersed in 4% PFA for 40 min at

194 RT. For frozen cryosections, the eyecups were dehydrated in 10% sucrose, followed

195 by 20%, 30% sucrose, embedded in OCT compounds, frozen, and cut as a 10-μm-

196 thick section. For retinal flat mounts, the retinas were mounted and dissected into a

197 four-leaf clover shape. The superior leaves were labeled by the preservation of the

198 surrounding retinal pigment epithelium and dissected into the largest piece for

199 orientation. The tissues were incubated with primary antibodies (rabbit anti-PLSCR1,

200 1:200; rabbit anti-RBPMS, 1:300; mouse anti-Brn3a, 1:500; goat anti-Iba1, 1:100; rat

201 anti-CD68, 1:300) overnight (cryosections) or for 72 h (retinal flat mounts) at 4 °C. After

202 washing in PBS, tissues were incubated with secondary antibodies (1:500) for 2 h at

203 RT and counterstained with DAPI (1:2000). Six images were captured at 300 μm from

204 the optic nerve head of each cryosection, while three images were captured from

205 central to peripheral regions in four quadrants of each retina (Fig. 4C). The whole

206 retinal mount and representative images of RBPMS labeled RGCs were acquired by a

207 Zeiss Axio Observer Inverted Microscope (TissueGnostics, Austria) running the

208 TissueFAXS 7.0 software with a 20 × objective. Orientation was indicated with S

209 (superior), I (inferior), N (nasal), and T (temporal) axes (Fig. 4D).

210

211 **Phosphatidylserine (PS) exposure assay**

212 *In vitro*, we performed polarity-sensitive annexin-based biosensor (pSIVA-IANBD,

213 Novus Biologicals, USA) in the calcium-dependent states, which can bound to

214 apoptosis cells and be detected by fluorescence. Before commencement of the

215 experiments, cells were washed twice with desktop fluid and supplemented with 2 mM

216 $CaCl_2$ in desktop fluid warmed to 37 °C for 10 min. pSIVA-IANBD and propidium iodide

217 (PI) were added and incubated in a dark condition at 37 °C for 5 min according to the

218 manufacturer's instructions. The PS on the extracellular face of plasma membrane

219 were binding by pSIVA, and the damage or necrotic cells were detected by PI. Hoechst

220 (Invitrogen, Thermo Fisher Scientific, USA) reagent was added to stain cell nuclear

221 stained. We then track the progression and timing of PLSCR1 effect on RPCs

222 apoptosis by live-cell imaging. To visualize PS exposure *in vivo*, mice were

223 anesthetized and injected 1.5 μl pSIVA solution into the vitreous one day after AOH.

224   The eyes were collected 2 h after pSIVA injection and fixed with 4% PFA for 20 min.

225   The retinal flat mounts were immediately observed by a confocal scanning microscope.

226

227   **TUNEL staining**

228   To perform TUNEL staining of the retinal cryosections, the cryosections were dried and

229   permeabilized with 0.1% Triton-X100 in PBS for 30 min at RT. After PBS rinsing, the

230   sections were incubated in dark places with terminal deoxynucleotidyl transferase

231   dUTP nick-end labeling (TUNEL, *In situ* Cell Death Detection Kit, Roche Life Science,

232   Switzerland) reaction mixture for 1 h at 37 °C and subsequently incubated with 0.1%

233   DAPI for 10 min. For the retinal flat mounts, 30 µl mixture per retina was used for

234   incubation for 2 h at RT in dark places before secondary antibodies incubation. The

235   images were captured with a confocal microscope as above described.

236

237   **Dihydroethidium (DHE) staining**

238   The 10-µM thick retinal cryosections from different experimental groups were taken to

239   room temperature and then covered with a 10 µM DHE solution (Invitrogen). The slides

240   were incubated in a light-protected humidified incubator at 37 °C for 30 min. Sections

241   were mounted with Fluoromount-G and covered with coverslips. Images were taken

242   using an LSM800 confocal scanning microscope.

243

244   **Histological assessment**

245   The procedure of histologic sections was prepared as described previously.[17] Briefly,

246   animals were sacrificed on the fifth day after AOH. A suture was placed on the edge of

247   of the inferior conjunctiva to identify the inferior portion of the eye. Eyes were

248   enucleated and fixed in FAS eye fixation solution (Servicebio Technology, China)

249   overnight at RT. After dehydrated in an ethanol series, eyeballs were embedded in

250   paraffin, cut in 4-μm sections through the suture and at the point of the optic nerve

251   head, and mounted on glass slides. Histology sections were stained with hematoxylin

252   and eosin (H&E). The microscopic image of each section was captured at 1 mm on

253   both sides from the optic disc and the thickness of the whole and each layer of the

254   retina were measured using Image J software.

255   The axon damage of RGCs was evaluated by toluidine blue (TB) staining on the

256   seventh day post AOH. After 4% PFA perfusion, the mouse optic nerves were cut

257   approximately 1 mm behind the globe, fixed by 2.5% glutaraldehyde for 2 h at RT, and

258   transferred to 4 °C overnight. Followed by washing with phosphate buffer, optic nerves

259   were placed in 1% OsO_4 for 2 h at RT and dehydrated with a series of ethanol and

260   isoamyl acetate. The nerves were then embedded in epoxy medium, cut sections at 1

261   μm with an ultramicrotome, and enhanced with osmium tetroxide-induced myelin

262   staining using 1% TB. Optic nerve was observed under light microscopy and the axon

263   damage was assessed using a semiquantitative optic nerve grading scheme in

264   accordance with previous studies.[18,19]

265

266   **Image analysis**

267   The number of interested cells (RGCs, microglia, and apoptosis cells) from each field

268   was counted using Image J software (LOCI, University of Wisconsin, USA) to obtain

269   the average quantification. Areas of immunopositivity (pSIVA, DHE, and CD68) were

270   derived by thresholding images captured under uniform imaging conditions. The unit

271   of each visual field used in statistics was under 20 × objective of an LSM800 confocal

272   scanning microscope (319.45 × 319.45 $μm^2$ per field).

273

274 Quantitative real-time reverse transcription-polymerase chain reaction (RT-PCR)

275 and quantitative PCR (qPCR)

276 Total RNA was extracted from retina samples using TRIzol™ reagent, and the final

277 concentration was quantified with a Nanodrop spectrophotometer (ND-1000;

278 NanoDrop Technologies, USA). Next, cDNA was synthesized with a qPCR RT Kit

279 (TOYOBO, Japan). The cDNA was then diluted with SYBR Green Supermix (Bio-Rad)

280 and was analyzed by qPCR for changes in gene expression. GAPDH mRNA was used

281 as an internal control. The primer sequences are listed in Supplementary Information.

282 Each cDNA sample was run in triplicate on Lightcycler 480 system PCR system

283 (Roche), superimposed on a standard curve to determine absolute transcript quantities.

284 The relative mRNA expression levels were calculated with the $2^{-\triangle\triangle Ct}$ method as in

285 previous research.[20] Data were analyzed using Bio-Rad CFX manager software.

286

287 RNA-seq analysis

288 The RNA-seq analysis was conducted by Berry Genomics Corporation (Beijing, China)

289 as our previous study.[21] RNA was extracted from the retinas of WT and TG-PLSCR1

290 mice with AOH treatment. A total amount of 1 µg RNA per sample was used as input

291 material. Sequencing libraries were generated using NEBNext® Ultra™ RNA Library

292 Prep Kit for Illumina® (NEB, USA) following the manufacturer's recommendations, and

293 index codes were added to attribute sequences to each sample. The clustering of the

294 index-coded samples was performed on a cBot Cluster Generation System using

295 TruSeq PE Cluster Kit v3-cBot-HS (Illumia). Then the library preparations were

296 sequenced on an Illumina NovaSeq platform and 150 bp paired-end reads were

297 generated. Clean data with high quality after processed raw data were aligned with

298 TopHat (v2.0.11) to the mouse genome (GRCm38/mm10). HTSeq v0.6.1 was used to

299 count the reads numbers mapped to each gene. Ingenuity pathway analysis (IPA)

300 (Qiagen Inc., Hilden, Germany) software was applied to analyze each sample's

301 expression values and detect significant differences in gene transcript expression

302 between groups. Sequences have been deposited in the NCBI Gene Expression

303 Omnibus (GEO) database (https://www.ncbi.nlm.nih.gov/geo/). The GEO accession is

304 GSE186750.

305

306 **Statistical analysis**

307 SPSS software (version 21.0; IBM SPSS Inc., USA) and GraphPad Prism (version 9.0;

308 GraphPad Inc., USA) were used for statistical analysis and graphics. The summarized

309 data were expressed as mean ± SD obtained from at least three independent

310 experiments. The differences between different groups were calculated by the two-

311 tailed Student's t-test. Statistical significance was defined as $P < 0.05$. NS indicates P

312 0.05, * indicates $P < 0.05$, ** indicates $P < 0.01$, and *** indicates $P < 0.001$.

313

314 **Results**

315 **Overexpressed PLSCR1 leads to its translocation in RPCs**

316 To verify the PLSCR1 expression in RPCs, we evaluated the protein expression level

317 of PLSCR1 in the blank group, pAd-NC group, and pAd-PLSCR1 group by Western

318 blot. Compared with the blank group, the expression of PLSCR1 was significantly

319 increased in the pAd-NC and pAd-PLSCR1 groups, especially in the pAd-PLSCR1

320 group (Fig. 1A, B). Then we performed immunostaining of PLSCR1 to investigate its

321 subcellular location in RPCs. In the blank and pAd-NC group, PLSCR1 was expressed

322   in the nucleus, cytoplasm, and cytomembrane of RPCs; whereas in the pAd-PLSCR1

323   group, PLSCR1 was not expressed in the nucleus but mainly localized in the cytoplasm

324   and cytomembrane (Fig. 1C). These findings showed that a much higher expression

325   of PLSCR1 would trigger its translocation from the nucleus to the cytoplasm and

326   cytomembrane in RPCs.

327

328   **PLSCR1 regulates PS exposure, cell apoptosis, and ROS generation in RPCs**

329   As PLSCR1 can process PS exposure as an immune response to viral infection,[22,23]

330   we use pSIVA, a fixable green fluorescent polarity sensitive indicator of viability and

331   apoptosis, to bind exposure PS and PI to probe death cells to evaluate the effect of

332   PLSCR1 on RPCs function. In the blank group, few RPC was detected with pSIVA/PI

333   fluorescence signal. The pSIVA/PI signals were significantly augmented in the virus-

334   infected groups, of which the pAd-PLSCR1 RPCs demonstrated more striking

335   fluorescence signals (Fig. 2A).

336   We then used flow cytometry of annexin V-FITC/PI to detect the rate of cell apoptosis

337   and death on RPCs. Consistently, RPCs treated with pAd-PSLCR1 had the highest

338   degree of cell apoptosis among the three groups (Fig. 2A, B). The early and late

339   apoptotic ratio in the blank group was 6.7% and 12.6% in the pAd-NC treated group,

340   while the percentage of apoptotic cells increased to 19.2% in the pAd-PLSCR1 group

341   (Fig. 2C). For further study, we detected the ROS generation by flow cytometry using

342   DCFH-DA. Compared with the blank group, cytosolic ROS production was significantly

343   elevated in the pAd-NC and pAd-PSLCR1 groups. Among them, the highest cytosolic

344   ROS level was observed in the pAd-PSLCR1 treated RPCs (Fig. 2D, E).

345   Using RNA interference to knock down PLSCR1 expression in RPCs (Fig. S2), we

346   then investigated whether PLSCR1 inhibition could ameliorate RPCs damage under

347   OGDR conditions. As an *in vitro* model mimicking AOH, OGDR treatment could

348   enhance pSIVA/PI fluorescence signal, cell apoptosis rate, and ROS accumulation in

349   RPCs. PLSCR1 inhibition by si-PLSCR1 substantially alleviated damage and death of

350   RPCs (Fig. S3). From the above results, we demonstrate that PLSCR1 regulates PS

351   exposure, cell apoptosis, and ROS generation in RPCs.

352

353   **Upregulated PLSCR1 contributes to its translocation in the retina and optic**

354   **nerve of transgenic PLSCR1 (TG-PLSCR1) mice**

355   To explore the roles of PLSCR1 in retinal degeneration, TG-PLSCR1 mice were

356   generated using a cDNA coding human *PLSCR1* gene transferred into mouse embryos.

357   Increased expression of PLSCR1 was verified by Western blot in the TG-PLSCR1 mice

358   retina (Fig. 3A, B). Then, we use immunostaining of PLSCR1 to examine its distribution

359   in mice retinas. In the retina of wild-type (WT) mice, PLSCR1 was mainly expressed in

360   the GCL and inner nuclear layer (INL). However, in the retina of TG-PLSCR1 mice,

361   PLSCR1 was not only expressed in the GCL and INL, but also expressed in the retinal

362   nerve fiber layer (RNFL), IPL, OPL, and outer nuclear layer (ONL). Also, in the retina

363   and optic nerve of wild-type (WT) mice, PLSCR1 was mainly expressed in the nucleus.

364   Whereas in the retina and optic nerve of TG-PLSCR1 mice, PLSCR1 was expressed

365   in the nucleus and cytoplasm (Fig. 3C).

366   We also examined the distribution of PLSCR1 in the brain and liver tissues from WT

367   and TG-PLSCR1 mice. In WT mice, PLSCR1 was located in the cell nucleus of brain

368   and liver. In TG-PLSCR1 mice, PLSCR1 was expressed in both nucleus and cytoplasm

369   in brain cells, whereas it was translocated to cytoplasm and cytomembrane in liver

370   cells (Fig. S4). These findings demonstrate that overexpressed PLSCR1 contributes

371   to its translocation at the subcellular and tissue level.

372

373   **Overexpression of PLSCR1 aggravates RGCs damage and death after acute**

374   **ocular hypertension (AOH**

375   As the expression of PLSCR1 is elevated in neurons in the cerebral ischemia

376   condition,[12] we thus investigated whether PLSCR1 was involved in the glaucomatous

377   damage by detecting its transcriptional expression in the AOH and ONC model. Our

378   finding revealed that the mRNA level of PLSCR1 significantly increased after treatment

379   (Fig. S5), suggesting that PLSCR1 might be a potential manipulator of retinal injury

380   and neuron death.

381   To identify the effects of PLSCR1 in the glaucomatous retina, we performed AOH

382   treatment in both WT and TG-PLSCR1 mice to assess the pathological change. The

383   thickness of each layer of retina, number of RGCs, and axon damage were evaluated.

384   Before AOH treatment, the morphology of the retina and optic nerve exhibited no

385   difference between WT and TG-PLSCR1 mice (Fig. 4A, F). However, compared with

386   WT mice, TG-PLSCR1 mice showed the whole retinal thickness had dramatically

387   decreased after AOH, especially in the RNFL, IPL, and INL (Fig. 4A, B). Also, the

388   number of RBPMS labeled RGCs markedly decreased in TG-PLSCR1 mice (Fig. 4D,

389   E). TB staining of optic nerve showed TG-PLSCR1 mice had much severer axon

390   damage of RGCs after AOH, assessed by semiquantitative grading (Fig. 4, G).

391   Altogether, these findings show that PLSCR1 exerts deleterious effects on the

392   glaucomatous retina and optic nerve.

393

394   **Elevated PLSCR1 facilitates PS exposure, cell apoptosis, and higher ROS**

395   **production in RGCs after AOH treatment**

396   Taken the overexpressed PLSCR1 promoted PS exposure, apoptosis, and cytosolic

397   ROS in RPCs, we explored whether PLSCR1 overexpression had a similar effect in

398   RGCs of AOH-treated retina. Using pSIVA to label exposed PS, we demonstrated an

399   increased pSIVA signal in GCL one day after AOH, and TG-PLSCR1 mice show a

400   higher level of pSIVA-immunopositivity than WT mice (Fig. 5A, D). Then we used

401   TUNEL staining and DHE to detect cytosolic apoptosis, and ROS in the AOH retinas,

402   respectively. The results showed a significant increase in the number of TUNEL

403   labeled apoptotic cells in the retinas one day after AOH treatment (Fig. 5C). More

404   apoptotic cells were observed in the GCL and INL of TG-PLSCR1 mice than those in

405   the WT mice (Fig. 5C, F). ROS production of the retinas was also assessed on the first

406   days after AOH. Notably, the retinas of TG-PLSCR1 mice with AOH treatment

407   exhibited the highest ROS level (Fig. 5B, E). Our findings indicate overexpression of

408   PLSCR1 aggravates PS exposure, cell apoptosis, and ROS level of RGCs in

409   glaucomatous damage.

410

Overexpressed PLSCR1 promotes activated microglia with increased phagocytosis, M1 polarization, and pro-inflammatory cytokines secretion

On the third day after AOH, we observed the retinal microglia infiltrating the GCL had morphology changed, from ramified shape to ameboid or rod shape (Fig. 6A). Then we performed immunostaining of Iba1 and CD68 to evaluate the number and phagocytic function of microglia, respectively. Our results showed that the number of microglia had no difference between WT and TG-PLSCR1 groups before treatment, yet the TG-PLSCR1 retinas have more microglia compared with the WT retinas after AOH (Fig. 6A, B). CD68 is a lysosome-associated membrane protein and scavenger receptor, and a marker for M1 type microglia.[24,25] In both WT and TG-PLSCR1 retinas, the expression of CD68 increased markedly in the GCL co-localized with Iba1 three days after AOH and the AOH-treated TG-PLSCR1 group exhibited a much higher immunopositivity level (Fig. 6A, C).

To assess M1 and M2 microglia polarization, we used a qPCR screen to determine gene expression changes in the retina of AOH-treated WT and TG-PLSCR1 mice. The mRNA level of M1 type microglia markers, such as TNF- , iNOS, and CD86, were distinctly upregulated in the AOH-treated TG-PLSCR1 group, but the mRNA levels of CCL-3 and CCL-5 showed no significant difference (Fig. 6D). The mRNA level of M2 type microglia markers, such as IL-10, YM-1, and CD206, had no significant difference between the two groups (Fig. 6E).

To gain better insight into the pathological neuroinflammation caused by PLSCR1,

432 we performed RNA-seq analysis on retinal tissue from WT and TG-PLSCR1 mice with

433 AOH treatment. As the PLSCR1 pathway has been reported to be involved in microglial

434 activation in neuroinflammation, we investigated the microglia associated molecules

435 and found that the mRNA level of genes in the pathway of immune system process,

436 response to stimulus, cytokine production, response to stress, and inflammatory

437 response were notably upregulated in AOH-treated TG-PLSCR1 mice (Fig. 6F). qPCR

438 validated the gene expression of RNA-seq (Fig. 6G). These data indicate that

439 overexpression of PLSCR1 enhances the inflammatory response in AOH injury by

440 facilitating microglia to exhibit an active state, phagocytic function, and M1 polarization.

441

442 **PLSCR1 facilitates clearance of apoptotic RGCs by microglia phagocytosis after**

443 **AOH**

444 According to the above results, the presence of an "eat-me" signal on RGCs and the

445 expression of phagocytic molecules in activated microglia suggests that microglial

446 phagocytosis of RGCs may contribute to RGCs injury and death. To investigate and

447 confirm the interaction between microglia with RGCs, we performed Iba1, TUNEL, and

448 RBPMS immunostaining to label microglia and apoptotic RGCs, respectively. On the

449 third day after AOH when microglia infiltrated the GCL, we observed that Iba1 labeled

450 activated microglia contained DAPI labeled cells that were immunopositive for TUNEL

451 and RBPMS, confirming the microglial engulfment of apoptotic RGCs in both WT and

452 TG-PLSCR1 retinas with AOH treatment (Fig. 7A–C). Assessment of the number of

453 TUNEL- and Brn3a-positive cells, as well as TUNEL-, Brn3a-, and Iba1-positive cells,

454 revealed that TG-PLSCR1 AOH-treated retinas showed significantly more apoptotic

455 RGCs and phagocytosed apoptotic RGCs than WT AOH-treated retinas (Fig. 7D).

19

456   Our results indicate that PLSCR1 promotes RGCs death and clearance by microglial

457   phagocytosis and provide direct evidence of intercellular interaction of activated

458   microglia and apoptotic RGCs in retinal neurodegeneration (Fig. 8).

459

460   **Discussion**

461   In the current study, we provide evidence that PLSCR1 is involved in the interactions

462   between microglia and RGCs, the secondary nerve cells of retina. PLSCR1 promotes

463   PS exposure, cell apoptosis, and ROS generation *in vitro* and *in vivo*. Upregulation of

464   PLSCR1 in the AOH-treated retina aggravates M1 type microglia activation and

465   phagocytosis of RGCs.

466   Accumulating studies showed that retinal microglia activated and neuroinflammation

467   occurred in the glaucomatous retina, resulting in retinal injury and RGCs death.[5,26-29]

468   Several genes and signaling pathways were found participating in the activation of

469   retinal microglia and RGC pathogenesis, such as CX3CR1, nucleotide-binding leucine-

470   rich repeat-containing receptor (NLR) family, Toll-like receptor (TLR) pathway, and

471   Jak-Stat pathway.[27,28,30-32] However, the direct intercellular interaction between retinal

472   microglia and damaged RGCs is unrevealed.

473   Phospholipid scramblase activity is involved in the collapse of phospholipid

474   asymmetry at the plasma membrane leading to the externalization of PS, which

475   provides a signal for the recruitment of macrophages or microglia to bind to and engulf

476   the apoptotic cells.[33] PLSCR, TMEM16, and XKR family members are specific

477   phospholipid scramblases that contribute to neurodegeneration. PLSCR1 has been

478 found to increase after ischemia injury and modulate microglia-mediated virus infected

479 cell clearance in CNS.[12,13] PLSCR3, localized in the mitochondrial membrane, is

480 associated with neuronal vulnerability to brain ischemia.[34,35] Deficiency of TMEM16F

481 could relieve the microglial phagocytosis in the pathogenesis of neuropathic pain and

482 cerebral ischemia.[36,37] XKR8, a caspase-activated scramblase, is implicated in

483 regulating bipolar cell death and axon clearance.[38,39] Also, rhodopsin and other G

484 protein-coupled receptors (GPCRs) are constitutively active as phospholipid

485 scramblases in neurons.[40,41] Located on the membrane of photoreceptor disc,

486 rhodopsin is thought to play a role in re-modelling cell membranes and its constitutive

487 activation will lead to retinal degenerations.[41,42] The titer of anti-rhodopsin antibodies

488 was found high in normal tension glaucoma patients' serum.[43,44] A Genome-wide

489 association study identifies phospholipid scramblase activity and phospholipid

490 scrambling pathways possibly correlate with high IOP and glaucoma in Westerners.[45]

491 Whereas, the specific role of phospholipid scramblase underlying glaucoma

492 pathogenesis remains unidentified.

493 Taken the essential role of PLSCR1 in the recognition and clearance of stressed

494 cells by microglia in the CNS, we investigate the function and potential mechanism of

495 PLSCR1 in glaucoma pathogenesis and attempt to clarify the intercellular interaction

496 between microglia and stressed RGCs.

497 In leukemic cells and breast cancer cells, endogenous PLSCR1 is mainly located in

498 the cytoplasm, and it traffics to the nuclear under some conditions.[46,47] Different from

499 the distribution in leukemic cells and breast cancer cells, endogenous PLCSR1 is

500 distributed in the whole cell of RPCs, and overexpression of PLSCR1 leads to its

501 translocation from the nucleus to the cytoplasm and cytomembrane. In the retina,

502 endogenous PLSCR1 is located in the cell nucleus of GCL and INL, whereas

503 overexpression leads to its distribution in the cell nucleus and cytoplasm of RNFL, IPL,

504 OPL, and ONL. As the distribution of PLSCR1 in neurons has not been reported

505 previously, our study suggests that PLSCR1 might exhibit different functions with the

506 variation of distribution and expression level after overexpression in neurons.

507 In many pathological conditions, the intracellular calcium homeostasis is disrupted

508 and subsequently the calcium-mediated signaling cascades activate. PLSCR1 can be

509 activated in the presence of increased cellular calcium and enhances IP3R expression,

510 in turn, influencing intracellular calcium homeostasis.[48] Both pAd-NC and pAd-

511 PLSCR1 infection to RPCs can upregulate PLSCR1 expression, PS exposure, cell

512 apoptosis, and ROS generation, while overexpressed PLSCR1 exacerbates these

513 effects. The virus infection of RPCs can be taken as a stimulus, which elevates the

514 expression of PLSCR1 by disrupting intracellular homeostasis, such as the induction

515 of ROS and the activation of apoptotic signals, thus causing PS exposure.

516 Overexpression of PLSCR1 aggravates the intracellular calcium dysregulation and

517 thereby exerts further deleterious effects. Inhibition of PLSCR1 in the OGDR model,

518 nevertheless, could attenuate the RPC damage and apoptosis.

519 In the mouse retina, AOH and ONC treatment lead to upregulated expression of

520 retinal PLSCR1. Although the distribution of retinal PLSCR1 was distinctly different

521 between WT and TG-PLSCR1 mice, there was no difference in retinal and optic nerve

522   morphology between two groups before AOH treatment. However, compared with WT

523   mice, the retinas of TG-PLSCR1 mice exhibited more deleterious damage with AOH

524   treatment. In TG-PLSCR1 mice, more PS exposure and TUNEL signals were observed

525   in the GCL on the first day after AOH treatment, and the number of RGCs and the

526   thickness of RNFL and GCL were significantly decreased on the fifth day after AOH

527   treatment. Axon damage was much severer in TG-PLSCR1 than controls in the AOH

528   model as well. These findings indicate that PLSCR1 might be served as a stress-

529   responsive gene in glaucomatous neuropathy and overexpression of PLSCR1 will

530   promote the progression of RGC pathogenesis.

531   On the first day after AOH, the acute hypertension stimulation affected the RGC

532   function and initiated the apoptosis process, presenting as PS exposure and TUNEL

533   signal in the GCL. PS exposure occurred in RGCs can be induced by oxidative stress,

534   such as ROS, which then attracted and activated microglia translocating from the outer

535   layer to the GCL. Then the activated microglia infiltrated the GCL on the third day after

536   AOH with ameboid morphology and upregulation of phagocytic molecules, CD68.

537   Consequently, on the fifth day after AOH, the number of RGCs and the thickness of

538   RNFL and GCL were decreased. TG-PLSCR1 mice showed more serious damage

539   compared with WT mice, implicating that overexpression of PLSCR1 further

540   aggravates the pathological process.

541   Activated microglia can be divided into two major subtypes, M1 and M2 type.[24,49]

542   The markers of M1 polarization are mostly mediators of pro-inflammatory responses

543   whereas M2 markers are considered neuroprotective. It is known that the products of

544 M1 microglia can lead to RGCs death via proinflammatory and oxidative stress

545 pathways in the glaucomatous retina.[5,50] Here, M1 types of microglia were significantly

546 increased in the TG-PLSCR1 retinas than WT in the AOH model, whereas there was

547 no difference in the M2 types of microglia. These findings indicated that overexpressed

548 PLSCR1 predominantly promotes retinal microglia polarization towards the M1

549 phenotype in glaucomatous damage, which can be validated by upregulated

550 expression of microglia-mediated inflammation genes and complement cascade

551 components in the RNA-seq results.

552 There are still some apoptotic RGCs that are not phagocytosed by microglia in AOH-

553 treated retinas. We supposed that the rest of apoptotic RGCs without being

554 phagocytosed might be partially caused by the upregulated pro-inflammation cytokines,

555 such as TNF- and iNOS, secreted from M1 type activated microglia. More M1 type

556 microglial cells were activated by upregulated expression of PLSCR1, which will

557 subsequently trigger more severely retinal damage via phagocytosis and secreting pro-

558 inflammation cytokines.

559

560 **Conclusions**

561 In summary, we demonstrate that PLSCR1 is a key regulator in promoting RGCs

562 apoptosis and clearance by M1 type microglia, which lead to the retina and optic nerve

563 injury and visual function impairment. Our study points out the connection between

564 PLSCR1 and retinal microglia and their interactions with RGCs degeneration, which

565 will contribute to a better understanding of glaucoma pathogenesis and provide

566 potential therapeutic targets for the treatment of glaucomatous damage or other RGC-

567 related neurodegeneration.

568

569 ***Ethics declaration***

570 All the animals were treated in strict accordance with Animal Research and this study

571 was formally reviewed and approved by the Zhongshan Ophthalmic Center Animal

572 Care and Ethics Committee.

573 ***Conflict of interests***

574 The authors declare that they have no competing interests

575 ***Author contributions***

576 L.Z., L.L., Y.L., and K.Z.: Conceptualization, Supervision, Resources, Writing - review

577 & editing. L.Z., J.L., Q.L. and D.Z.: Investigation, Methodology, Visualization, Writing -

578 original draft. J.L., Q.L., D.Z. M.Z., T.M., B.S., Z.Y., C.L., W.X., L.Z., K.W., X.L., Y.L,

579 F.M., W.L., C.Z., M.L.: Investigation, Data curation, Formal analysis, Software. All

580 authors read and approved the final manuscript.

590   ***Acknowledgements***

591   We thank the staff of Core Facilities at State Key Laboratory of Ophthalmology,

592   Zhongshan Ophthalmic Center for technical support. We also gratefully acknowledge

593   the staff of the Laboratory Animal Center at State Key Laboratory of Ophthalmology,

594   Zhongshan Ophthalmic Center.

595   ***Data availability***

596   The datasets used and/or analyzed during the current study are available from the

597   corresponding author on reasonable request.

598

599

References

1. Davis BM, Crawley L, Pahlitzsch M, Javaid F, Cordeiro MF. Glaucoma: the retina and beyond. *Acta Neuropathol* . 2016;132(6):807-826.

2. Quigley HA. Glaucoma. *Lancet.* 2011;377(9774):1367-1377.

3. Skowronska-Krawczyk D, Zhao L, Zhu J, et al. P16INK4a upregulation mediated by SIX6 defines retinal ganglion cell pathogenesis in glaucoma. *Mol Cell.* 2015;59(6):931-940.

4. Silverman SM, Wong WT. Microglia in the retina: roles in development, maturity, and disease. *Annu Rev Vis Sci.* 2018;4:45-77.

5. Baudouin C, Kolko M, Melik-Parsadaniantz S, Messmer EM. Inflammation in Glaucoma: from the back to the front of the eye, and beyond. *Prog Retin Eye Res.* 2021;83:100916.

6. Reichenbach A, Bringmann A. Glia of the human retina. *Glia.* 2020;68(4):768-796.

7. Zhao L, Zabel MK, Wang X, et al. Microglial phagocytosis of living photoreceptors contributes to inherited retinal degeneration. *EMBO Mol Med.* 2015;7(9):1179-1197.

8. Dal Monte M, Cammalleri M, Locri F, et al. Fatty acids dietary supplements exert anti-inflammatory action and limit ganglion cell degeneration in the retina of the EAE mouse model of multiple sclerosis. *Nutrients.* 2018;10(3):325.

9. Njie-Mbye YF, Kulkarni-Chitnis M, Opere CA, Barrett A, Ohia SE. Lipid peroxidation: pathophysiological and pharmacological implications in the eye. *Front Physiol.* 2013;4:366.

10. Darwich Z, Klymchenko AS, Kucherak OA, Richert L, Mély Y. Detection of apoptosis

27

622   through the lipid order of the outer plasma membrane leaflet. *Biochim Biophys Acta.*

623   2012;1818(12):3048-3054.

624   11. Brown GC, Neher JJ. Microglial phagocytosis of live neurons. *Nat Rev Neurosci.*

625   2014;15(4):209-216.

626   12. Rami A, Sims J, Botez G, Winckler J. Spatial resolution of phospholipid scramblase 1

627   (PLSCR1), caspase-3 activation and DNA-fragmentation in the human hippocampus

628   after cerebral ischemia. *Neurochem Int.* 2003;43(1):79-87.

629   13. Tufail Y, Cook D, Fourgeaud L, et al. Phosphatidylserine exposure controls viral innate

630   immune responses by microglia. *Neuron.* 2017;93(3):574-586.

631   14. Lamba DA, Karl MO, Ware CB, Reh TA. Efficient generation of retinal progenitor cells from

632   human embryonic stem cells. *Proc Natl Acad Sci U S A.* 2006;103(34):12769-12774.

633   15. Liu X, Liu Y, Jin H, et al. Reactive fibroblasts in response to optic nerve crush injury. *Mol*

634   *Neurobiol.* 2021;58(4):1392-1403.

635   16. Yu ST, Sun BH, Ge JN, et al. CRLF1-MYH9 interaction regulates proliferation and

636   metastasis of papillary thyroid carcinoma through the ERK/ETV4 axis. *Front*

637   *Endocrinol (Lausanne).* 2020;11:535.

638   17. Lian Q, Zhao M, Li T, et al. In vivo detecting mouse persistent hyperplastic primary

639   vitreous by Spectralis Optical Coherence Tomography. *Exp Eye Res.* 2019;181:271-

640   276.

641   18. Chauhan BC, Levatte TL, Garnier KL, et al. Semiquantitative optic nerve grading scheme

642   for determining axonal loss in experimental optic neuropathy. *Invest Ophthalmol*

643   *Vis Sci.* 2006;47(2):634-640.

644   19. Ebneter A, Casson RJ, Wood JP, Chidlow G. Microglial activation in the visual pathway in

645   experimental glaucoma: spatiotemporal characterization and correlation with

646   axonal injury. *Invest Ophthalmol Vis Sci.* 2010;51(12):6448-6460.

647   20. Yu ST, Zhong Q, Chen RH, et al. CRLF1 promotes malignant phenotypes of papillary

648   thyroid carcinoma by activating the MAPK/ERK and PI3K/AKT pathways. *Cell Death*

649   *Dis.* 2018;9(3):371.

650   21. Zhao M, Mei T, Shang B, et al. Defect of LSS disrupts lens development in

651   cataractogenesis. *Front Cell Dev Biol.* 2021;9:788422.

652   22. Yang J, Zhu X, Liu J, et al. Inhibition of Hepatitis B virus replication by phospholipid

653   scramblase 1 in vitro and in vivo. *Antiviral Res.* 2012;94(1):9-17.

654   23. Dong B, Zhou Q, Zhao J, et al. Phospholipid scramblase 1 potentiates the antiviral activity

655   of interferon. *J Virol.* 2004;78(17):8983-8993.

656   24. Franco R, Fernández-Suárez D. Alternatively activated microglia and macrophages in the

657   central nervous system. *Prog Neurobiol.* 2015;131:65-86.

658   25. Holness CL, da Silva RP, Fawcett J, Gordon S, Simmons DL. Macrosialin, a mouse

659   macrophage-restricted glycoprotein, is a member of the lamp/lgp family. *J Biol*

660   *Chem.* 1993;268(13):9661-9666.

661   26. Oikawa K, Ver Hoeve JN, Teixeira LBC, et al. Sub-region-specific optic nerve head glial

662   activation in glaucoma. *Mol Neurobiol.* 2020;57(6):2620-2638.

663   27. Lozano DC, Choe TE, Cepurna WO, Morrison JC, Johnson EC. Early optic nerve head glial

664   proliferation and Jak-Stat pathway activation in chronic experimental glaucoma.

665   *Invest Ophthalmol Vis Sci.* 2019;60(4):921-932.

666   28. Yang X, Luo C, Cai J, et al. Neurodegenerative and inflammatory pathway components

667   linked to TNF- /TNFR1 signaling in the glaucomatous human retina. *Invest*

668   *Ophthalmol Vis Sci.* 2011;52(11):8442-8454.

669   29. Yuan L, Neufeld AH. Activated microglia in the human glaucomatous optic nerve head.

670   *J Neurosci Res.* 2001;64(5):523-532.

671   30. Breen KT, Anderson SR, Steele MR, Calkins DJ, Bosco A, Vetter ML. Loss of fractalkine

672   signaling exacerbates axon transport dysfunction in a chronic model of glaucoma.

673   *Front Neurosci.* 2016;10:526.

674   31. Chen H, Deng Y, Gan X, et al. NLRP12 collaborates with NLRP3 and NLRC4 to promote

675   pyroptosis inducing ganglion cell death of acute glaucoma. *Mol Neurodegener.*

676   2020;15(1):26.

677   32. Chi W, Li F, Chen H, et al. Caspase-8 promotes NLRP1/NLRP3 inflammasome activation

678   and IL-1 production in acute glaucoma. *Proc Natl Acad Sci U S A.*

679   2014;111(30):11181-11186.

680   33. Kodigepalli KM, Bowers K, Sharp A, Nanjundan M. Roles and regulation of phospholipid

681   scramblases. *FEBS Lett.* 2015;589(1):3-14.

682   34. Dave KR, Bhattacharya SK, Saul I, et al. Activation of protein kinase C delta following

683   cerebral ischemia leads to release of cytochrome C from the mitochondria via bad

684   pathway. *PLoS One.* 2011;6(7):e22057.

685   35. Kowalczyk JE, Beresewicz M, Gajkowska B, Zabłocka B. Association of protein kinase C

686   delta and phospholipid scramblase 3 in hippocampal mitochondria correlates with

687   neuronal vulnerability to brain ischemia. *Neurochem Int.* 2009;55(1-3):157-163.

688 36. Zhang Y, Li H, Li X, et al. TMEM16F aggravates neuronal loss by mediating microglial

689   phagocytosis of neurons in a rat experimental cerebral ischemia and reperfusion

690   model. *Front Immunol.* 2020;11:1144.

691 37. Batti L, Sundukova M, Murana E, et al. TMEM16F regulates spinal microglial function in

692   neuropathic pain states. *Cell Rep.* 2016;15(12):2608-2615.

693 38. Sapar ML, Ji H, Wang B, et al. Phosphatidylserine externalization results from and causes

694   neurite degeneration in Drosophila. *Cell Rep.* 2018;24(9):2273-2286.

695 39. Kautzman AG, Keeley PW, Ackley CR, Leong S, Whitney IE, Reese BE. *Xkr8* modulates

696   bipolar cell number in the mouse retina. *Front Neurosci.* 2018;12:876.

697 40. Li T, Chiou B, Gilman CK, et al. A splicing isoform of GPR56 mediates microglial synaptic

698   refinement via phosphatidylserine binding. *EMBO J.* 2020;39(16):e104136.

699 41. Goren MA, Morizumi T, Menon I, et al. Constitutive phospholipid scramblase activity of

700   a G protein-coupled receptor. *Nat Commun.* 2014;5:5115.

701 42. Ernst OP, Menon AK. Phospholipid scrambling by rhodopsin. *Photochem Photobiol Sci.*

702   2015;14(11):1922-1931.

703 43. Romano C, Barrett DA, Li Z, Pestronk A, Wax MB. Anti-rhodopsin antibodies in sera from

704   patients with normal-pressure glaucoma. *Invest Ophthalmol Vis Sci.*

705   1995;36(10):1968-1975.

706 44. Romano C, Li Z, Arendt A, Hargrave PA, Wax MB. Epitope mapping of anti-rhodopsin

707   antibodies from patients with normal pressure glaucoma. *Invest Ophthalmol Vis Sci.*

708   1999;40(6):1275-1280.

709 45. Blue Mountains Eye Study (BMES); Wellcome Trust Case Control Consortium 2 (WTCCC2).

710   Genome-wide association study of intraocular pressure identifies the GLCCI1/ICA1

711   region as a glaucoma susceptibility locus. *Hum Mol Genet.* 2013;22(22):4653-4660.

712   46. Huang P, Liao R, Chen X, et al. Nuclear translocation of PLSCR1 activates STAT1 signaling

713   in basal-like breast cancer. *Theranostics.* 2020;10(10):4644-4658.

714   47. Li H, Xu J, Zhou Y, et al. PLSCR1/IP3R1/Ca(2+) axis contributes to differentiation of

715   primary AML cells induced by wogonoside. *Cell Death Dis.* 2017;8(5):e2768.

716   48. Zhou Q, Ben-Efraim I, Bigcas JL, Junqueira D, Wiedmer T, Sims PJ. Phospholipid

717   scramblase 1 binds to the promoter region of the inositol 1,4,5-triphosphate

718   receptor type 1 gene to enhance its expression. *J Biol Chem.* 2005;280(41):35062-

719   35068.

720   49. Tang Y, Le W. Differential roles of M1 and M2 microglia in neurodegenerative diseases.

721   *Mol Neurobiol.* 2016;53(2):1181-1194.

722   50. Bosco A, Romero CO, Breen KT, et al. Neurodegeneration severity can be predicted from

723   early microglia alterations monitored in vivo in a mouse model of chronic glaucoma.

724   *Dis Model Mech.* 2015;8(5):443-455.

725

726

727 **Figure 1** Overexpressed PLSCR1 leads to its translocation in RPCs.

728 **(A)** Western blot shows the protein expression of PLSCR1 expression in RPCs without

729 pAd treatment (Blank), and RPCs treated with pAd-NC and pAd-PLSCR1. **(B)** Statistic

730 analysis of the relative protein expression of PLSCR1 normalized to -Tubulin in RPCs

731 demonstrates the expression increases in pAd-NC and pAd-PLSCR1 groups. Two-

732 tailed Student's *t*-test (*n* = 3 for each experiment). *$P < 0.05$, ***$P < 0.001$. Data are

733 mean ± SD. **(C)** Immunofluorescence shows that PLSCR1 locates in the nucleus,

734 cytoplasm, and cytomembrane in RPCs without pAd treatment and RPCs infected with

735 pAd-NC, while it was translocated from the nucleus to the cytoplasm and

736 cytomembrane with enhanced immunofluorescence in RPCs infected with pAd-

737 PLSCR1. Scale bars, 20 μm.

738

739 **Figure 2** Overexpressed PLSCR1 promotes phosphatidylserine (PS) exposure, cell

740 apoptosis, and reactive oxygen species (ROS) generation in RPCs. **(A)**Live-cell

741 imaging using the polarity-sensitive phosphatidylserine-binding dye, annexin-based

742 fluorescent indicator polarity sensitive indicator of viability and apoptosis (pSIVA) and

743 propidium iodide (PI) shows the PS exposure and cell death increases in RPCs treated

744 with pAd-NC and pAd-PLSCR1. Scale bars, 100 μm. **(B)** Apoptosis of RPCs (Blank),

745 and RPCs treated with pAd-NC or pAd-PLSCR1 were evaluated by Annexin V-FITC

746 and PI by flow cytometry. **(C)** Quantification analysis of the early and late apoptotic rate

747 in RPCs (Blank), and RPCs treated with pAd-NC or pAd-PLSCR1. **(D)** The production

748 of ROS using 2',7'-dichlorodihydrofluorescein diacetate (DCFH-DA) is detected by flow

749 cytometry. **(E)** Statistic analysis of the mean intensity of DCFH-DA fluorescence value

750 in different groups shows PLSCR1 significantly increased the ROS generation in RPCs.

751 **(A, B, D)** RPCs are infected with pAd-NC and pAd-PLSCR1 for 48 h. **(C, E)** Statistic

752   analysis shows two-tailed Student's *t*-test (*n* = 3 for each experiment). *P < 0.05, **P

753   < 0.01. Data are mean ± SD.

754

755   **Figure 3** Upregulated PLSCR1 contributes to its translocation in the retina and optic

756   nerve of TG-PLSCR1 mice. **(A)** Western blot results show the PLSCR1 protein

757   expression elevates in the retina of TG-PLSCR1 mice compared with WT. **(B)** Statistic

758   analysis of PLSCR1 normalized expression level. Two-tailed Student's *t*-test (*n* = 3 for

759   each experiment). ***P < 0.001. Data are mean ± SD.

760   **(C)** Immunofluorescence images of PLSCR1 in the retina and optic nerve of WT and

761   TG-PLSCR1 showed different expression and localization. Scale bars, 50 µm.

762

763   **Figure 4** Overexpression of PLSCR1 aggravates RGCs damage and death after AOH.

764   **(A)** H&E staining shows the thickness of retina in different groups. Scale bars, 20 µm.

765   **(B)** Statistic analysis shows the thickness of different layers of the retina significantly

766   decreased in AOH-treated TG-PLSCR1 mice. **(C)** Indicative map demonstrates that

767   three images (central, middle, and peripheral) were captured in every quadrant of the

768   whole mount retina. A total of 12 fields were assessed for each retina. **(D)**

769   Immunofluorescence images show that the number of RBPMS labeled RGCs (red)

770   decreased in the AOH-treated mice (5 days). The change is more pronounced in TG-

771   PLSCR1 mice. The upper row shows the density distribution of RGCs in the whole

772   mount retina (Scale bars, 1 mm). The lower row exhibits the magnified micrographs

773   from the middle region in the superior quadrant of the corresponding retinas (white box)

774   (Scale bars, 50 µm). **(E)** Statistic analysis shows the average survival RGCs numbers

775   from 12 fields per retina. **(F)** Toluidine blue staining images of optic nerve transverse

776   section demonstrate axon damage in the AOH-treated mice, manifesting reduced axon

777 density, myelin disruption, and fields with gliosis (Scale bars, 5 μm). **(G)** Statistic

778 analysis of axon damage grade shows TG-PLSCR1 mice have much severer axon

779 damage than WT mice. **(B, E, G)** Two-tailed Student's *t*-test (B and G: *n* = 4; E: *n* = 5

780 for each experiment). *$P < 0.05$, **$P < 0.01$, ***$P < 0.001$, and NS indicates difference

781 not significant. Data are mean ± SD. RNFL, retinal nerve fiber layer; GCL, ganglion cell

782 layer; IPL, inner plexiform layer; INL, inner nuclear layer; OPL, outer plexiform layer;

783 ONL, outer nuclear layer. S, superior; I, inferior; N, nasal; T, temporal.

784

785 **Figure 5** Elevated PLSCR1 facilitates PS exposure, cell apoptosis, and higher ROS

786 production after AOH treatment.

787 **(A–C)** Immunofluorescence images of annexin-based fluorescent indicator polarity

788 sensitive indicator of viability and apoptosis (pSIVA) in the ganglion cell layer **(A)**,

789 dihydroethidium (DHE) **(B)**, and TUNEL staining **(C)** shows that PS exposure, ROS

790 level, and retinal cell apoptosis markedly increased in TG-PLSCR1 retinas after AOH.

791 Scale bars, 50 μm. **(D–F)** Statistic analysis of pSIVA immunopositivity **(D)**, ROS level

792 **(E)**, and TUNEL staining cell number **(F)** shows two-tailed Student's *t*-test (*n* = 3 for

793 each experiment). *$P < 0.05$, **$P < 0.01$, ***$P < 0.001$, and NS indicates difference not

794 significant. Data are mean ± SD.

795

796 **Figure 6** Overexpressed PLSCR1 promotes activated microglia with increased

797 phagocytosis, M1 polarization, and pro-inflammatory cytokines secretion. **(A)**

798 Immunofluorescence images of retinal flat mounts show microglia infiltrating the

799 ganglion cell layer (GCL) with ameboid morphology and upregulation of the phagocytic

800 molecule marker CD68 (green) on the third day after AOH. The immunostaining of

801 CD68 (green) is co-localized within Iba1 labeled microglia (red). Scale bar, 50 μm.

802 **(B)** Statistic analysis shows the number of Iba1 labeled microglia increases after

803 treatment and more microglia activated in the GCL of TG-PLSCR1 mice compared with

804 WT mice. **(C)** Statistic analysis shows that the immunopositivity of CD68 was

805 significantly enhanced, demonstrating the microglial activation is much more

806 pronounced in the TG-PLSCR1 mice. **(D, E)** The mRNA of WT and TG-PLSCR1 mice

807 with AOH treatment are isolated from the mouse retinas. qPCR data show higher

808 mRNA levels of M1 type microglia markers (TNF-, iNOS, CD86, CCL2, CXCL10, IL-

809 1, and IL-6) in TG-PLSCR1 mice compared with WT mice; whereas the mRNA level

810 of M2 type microglia markers (IL-10, YM-1, TGF-, CD206, and Fizz-1) shows no

811 significant difference between groups. **(F)** RNA-seq analysis identifies significant

812 upregulated microglia-mediated inflammation gene transcripts suggesting a higher

813 level of microglial activation and microglial inflammatory response in TG-PLSCR1

814 retinas compared with controls. **(G)** qPCR analysis verifies the genes expression in

815 RNA-seq data. **(B–E, G)** Two-tailed Student's t-test (B and C: $n = 4$; D, E, and G: $n =$

816 6 for each experiment). $^{*}P < 0.05$, $^{**}P < 0.01$, $^{***}P < 0.001$ and NS indicates difference

817 not significant. Data are mean ± SD.

818

819 **Figure 7** PLSCR1 facilitates clearance of apoptotic RGCs by microglia phagocytosis

820 after AOH. **(A)** Retinal flat mounts from TG-PLSCR1 mice three days after AOH shows

821 more activated microglia and more apoptotic RGCs than WT AOH-treated mice.

822 Microglia labeled with Iba1 (purple), apoptotic cells labeled with TUNEL (green), and

823 RGCs labeled with RBPMS (red). Arrowhead indicates the apoptotic RGCs

824 phagocytosed by microglia. Scale bar, 20 μm. **(B, C)** Three-dimensional images

825 reconstruction of the indicated area (white box in A) confirm the apoptotic RGCs inside

826 the soma of microglia. Scale bar, 2 μm. **(D)** Statistic analysis for TUNEL labeled RGCs

36

827 with or without microglial phagocytosis in WT and TG-PLSCR1 mice. Two-tailed

828 Student's *t*-test (*n* = 3 for each experiment). ***P* < 0.001. Data are mean ± SD.

829

830 **Figure 8** Schematic illustrating the activated retinal microglia contribute to RGCs death

831 by phagocytosis and secreting pro-inflammatory cytokines in AOH, and

832 overexpression of PLSCR1 exacerbates this pathological process. In the AOH retina,

833 RGCs become damaged (orange box) marked by exposed phosphatidylserine (PS),

834 TUNEL, and reactive oxygen species (ROS) staining, which induce microglia

835 recruitment. Ramified microglia infiltrate the ganglion cell layer (GCL) three days after

836 AOH, showing ameboid morphology, upregulated phagocytic molecules (CD68), M1

837 phenotype activation markers (e.g., CD86 and CXCL10), and pro-inflammatory

838 cytokines (e.g., TNF- and iNOS). The activated microglia, on the one hand,

839 phagocytose a subset of TUNEL labeled RGCs (purple box); on the other hand,

840 additionally influence and potentiate the apoptotic route for RGCs death via pro-

841 inflammatory cytokines secretion, such as TNF- and IL-1 (grey box).

842 Overexpression of PLSCR1 in the AOH-treated eye increases the PS exposure,

843 apoptosis, and ROS generation of RGCs, and therefore intensifies microglia activation

844 in phagocytosis and pro-inflammatory cytokine production, which aggravates RGCs

845 clearance and death.

846

847

A

PLSCR1 35KD

β-Tubulin 55KD

B

Relative PLSCR1 protein levels

***

*

Blank   pAd-NC   pAd-PLSCR1

C   PLSCR1   DAPI   Merge

Blank

pAd-NC

pAd-PLSCR1

20μm